JACS
JOURNAL OF THE AMERICAN CHEMICAL SOCIETY
Article
pubs.acs.org/JACS

On the Origins of Nonradiative Excited State Relaxation in Aryl Sulfoxides Relevant to Fluorescent Chemosensing

Rahul S. Kathayat,[†] Lijun Yang,[‡] Tosaporn Sattasathuchana,[†] Laura Zoppi,[†] Kim K. Baldridge,[†,‡] Anthony Linden,[†] and Nathaniel S. Finney*[,†,‡]

[†]Department of Chemistry, University of Zurich, Winterthurerstrasse 190, CH-8057 Zurich, Switzerland
[‡]School of Pharmaceutical Science and Technology, Tianjin University, 92 Weijin Road, Nankai District, Tianjin, 300072, China

Supporting Information

ABSTRACT: We provide herein a mechanistic analysis of aryl sulfoxide excited state processes, inspired by our recent report of aryl sulfoxide based fluorescent chemosensors. The use of aryl sulfoxides as reporting elements in chemosensor development is a significant deviation from previous approaches, and thus warrants closer examination. We demonstrate that metal ion binding suppresses nonradiative excited state decay by blocking formation of a previously unrecognized charge transfer excited state, leading to fluorescence enhancement. This charge transfer state derives from the initially formed locally excited state followed by intramolecular charge transfer to form a sulfoxide radical cation/aryl radical anion pair. With the aid of computational studies, we map out ground and excited state potential energy surface details for aryl sulfoxides, and conclude that fluorescence enhancement is almost entirely the result of excited state effects. This work expands previous proposals that excited state pyramidal inversion is the major nonradiative decay pathway for aryl sulfoxides. We show that pyramidal inversion is indeed relevant, but that an additional and dominant nonradiative pathway must also exist. These conclusions have implications for the design of next generation sulfoxide based fluorescent chemosensors.

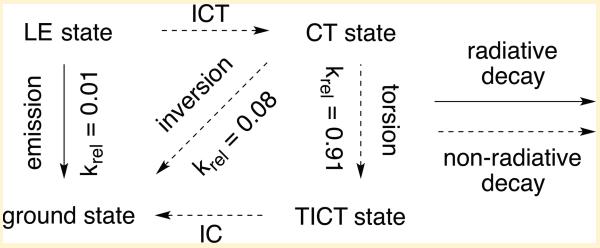

INTRODUCTION

Fluorescent chemosensors—small molecule probes that respond to reversible analyte binding by undergoing changes in fluorescence—are now widely used in the detection of nonfluorescent analytes in biological, medical, and environmental assays.[1] These probes are chiefly based on modulation of photoinduced electron transfer (PET) or intramolecular charge transfer (ICT), induced by nitrogen atom coordination.[2] Less common for small molecule probes are other signaling mechanisms, such as Förster resonance energy transfer (FRET), binding-induced conformational restriction, excited state proton transfer, and excimer formation.[2] The heavy reliance on nitrogen binding, while efficient and widely employed, suffers from drawbacks such as pH sensitivity and requisite placement of the recognition domain at anilinic or benzylic amine positions. These limitations provide motivation to discover alternative motifs for signaling, in order to broaden the range of strategies and structures for development of fluorescent chemosensors.[3−6]

To this end, we have reported a new approach employing aryl sulfoxides as the chemosensor signaling motif (**1a−e**; Chart 1).[7] Remarkable gains in fluorescence emission from pyrenyl sulfoxides were demonstrated to occur upon metal ion coordination (Figure 1), despite the very weak intrinsic affinity of sulfoxides for metal ions.[7−9]

The sensitivity to metal ions was shown to increase manyfold upon replacing the methyl group of **1a** with more strongly coordinating receptor units as in **1b−e**.[7] In addition, sulfoxide-based fluorophores were shown to function in aqueous media. Sulfoxides as a signaling motif, therefore, have potential for the development of useful metal ion responsive chemosensors.

Chart 1. Sulfoxide-Based Fluorescent Chemosensors 1a−e

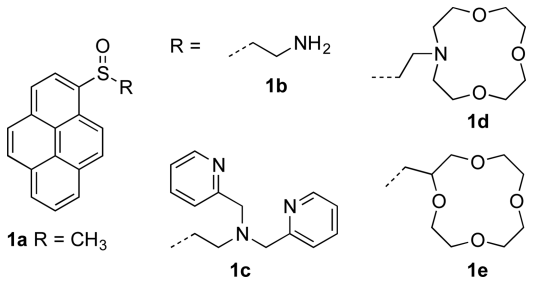

Before further expansion of this approach, it is essential to understand the mechanistic basis for fluorescence enhancement. Based on a combination of experimental and theoretical work we provide insight into the excited state processes of aryl sulfoxides, with particular emphasis on how these processes are perturbed by metal ion coordination.

RESULTS AND DISCUSSION

Structural and Optical Properties. The general optical properties of **1a** and the related molecules **1b−e** are very

Received: January 21, 2016
Published: November 3, 2016

DOI: 10.1021/jacs.6b00572
J. Am. Chem. Soc. 2016, 138, 15889−15895

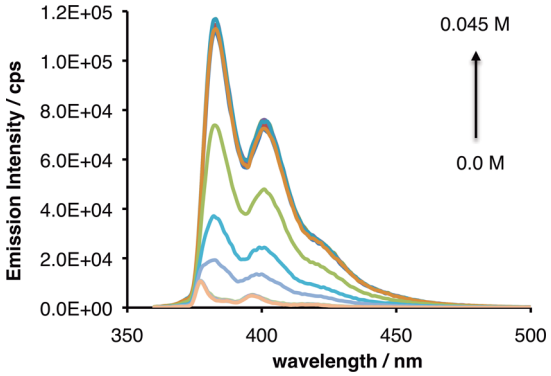

Figure 1. Titration of **1a** (10 μM in CH_3CN) with $ZnCl_2$.

similar to those of pyrene. The longer-wavelength absorption maxima of **1a–e** are slightly red-shifted, indicating variation of the π/π^* energetic separation as a consequence of the sulfoxide substituent (Figure S1).

The crystal structure of **1a** reveals that the S–O bond lies coplanar with the pyrene ring in the solid state (Figure S5). This could be taken as reflecting a favorable alignment of the pyrene π system with the bond formed between an O atom lone pair and an empty d orbital on S. (This S–O bonding is often—incorrectly—taken as being the "second bond" of a π bond between S and O.) In fact, while our optimized structure does not show perfect pyrene/S–O coplanarity, the dihedral angle between the S–O bond and the pyrene π system is quite small (ca. 20°; Figure S6), still consistent with conjugation, as evident from the molecular orbitals. Previous computational and experimental gas-phase and solution-phase studies indicate that, regardless of the minimum energy configuration, the barrier to rotation of the C_{aryl}–S(O) bond is very low, possibly <1 kcal/mol.[10] The conjugative interaction between the pyrene and the sulfoxide is thus weak enough that variation in the π/π^* energy gap could just as well result from inductive effects.[11]

The quantum yields of **1a–e** (Table 1) are very low, consistent with the previous reports for alky aryl sulfoxides.[7,12]

Table 1. Optical Properties of 1a–e[a,b]

compound	ε[c]	ϕ_f[d]
pyrene	54.0	0.32
1a	34.7	0.012
1b	31.1	0.009
1c	27.6	0.004
1d	28.5	0.003
1e	27.5	0.015

[a]All measurements made in CH_3CN. Emission spectra acquired at 10 μM, with excitation at the longest λ absorption maximum. [b]Longest λ absorption/emission maxima for pyrene: 335 nm/381 nm.[13] Longest λ absorption/emission maxima for **1a–e**: 349–350 nm/377–378 nm. [c]Units: 10^3 M^{-1} cm^{-1}. [d]Literature quantum yield for pyrene;[13] absolute quantum yields for **1a–e**.

These reports have shown that the low emission in aromatic sulfoxides is a consequence of nonradiative deactivation of the excited state, rather than variation in the rate of radiative decay.

Established Excited State Deactivation Pathways. The alkyl aryl sulfoxide nonradiative decay mechanism is dependent on the nature of the alkyl group attached to the sulfur atom. It is well-established that, for alkyl aryl sulfoxides bearing 2°/3° alkyl groups, the excited states deactivate by undergoing reversible fragmentation to form a sulfinyl/carbinyl radical pair.[12] It is accepted that aryl sulfoxides possessing a 1° alkyl group, such as **1a–e**, primarily deactivate via excited state photostereomutation at the tetrahedral sulfoxide center.[12,14,15] That is, the excited state energy is dissipated by pyramidal inversion of the sulfoxide. This has most convincingly been shown through labeling studies (Figure 2),[12e] where the major

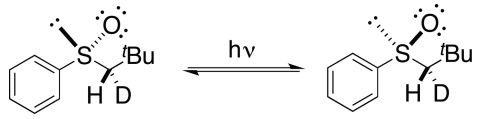

Figure 2. Photostereomutation of a labeled 1° alkyl/aryl sulfoxide.

photochemical product was that of pyramidal inversion in the singlet excited state, with negligible radical fragmentation. (The involvement of triplet states in this process has been excluded.)[12c,14]

As our fluorescent probes are all aryl sulfoxides bearing a 1° alkyl group, our studies have focused on the origin of excited state sulfoxide pyramidal inversion.

Racemization Studies. To begin, it was necessary to see whether enhanced fluorescence in the presence of metal ions was correlated with reduced pyramidal inversion. We studied the photoracemization of sulfoxide (*S*)-**1a** (Scheme 1) and observed that added metal ions do indeed influence this process (Figure 3).

Scheme 1. Synthesis of Sulfoxide (*S*)-1a

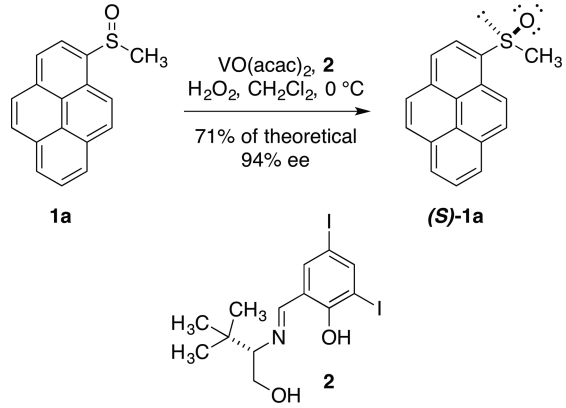

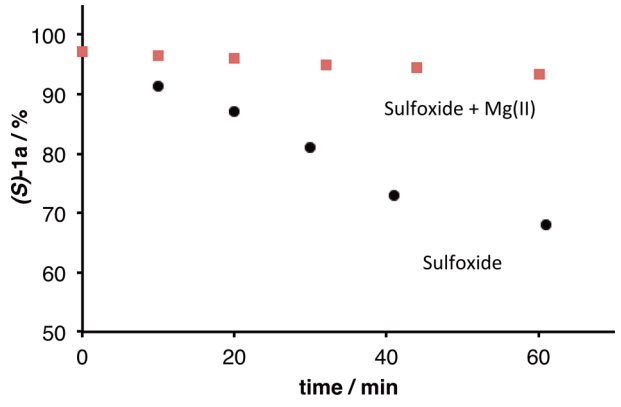

Figure 3. Photoracemization of (*S*)-**1a** (2.5 mM, CH_3CN), with and without added $Mg(ClO_4)_2$.

DOI: 10.1021/jacs.6b00572
J. Am. Chem. Soc. 2016, 138, 15889–15895

Enantiomerically enriched (*S*)-**1a** was obtained in 94% ee (97% (*S*)-**1a**) and acceptable yield by oxidative kinetic resolution of racemic **1a** using a chiral catalyst generated in situ from $VO(acac)_2$ and ligand **2** (Scheme 1).[16] The absolute configuration of (*S*)-**1a** was confirmed by single crystal XRD (Figure S5).[17]

Irradiation of 2.5 mM (*S*)-**1a** in CH_3CN was carried out, with and without excess (100 equiv) $Mg(ClO_4)_2$, in quartz cuvettes, irradiating with a TLC lamp.[17] Small samples were withdrawn at periodic intervals, and the enantiomeric composition was determined by HPLC on a chiral column (Figure S2). The two enantiomers of **1a** were found to be the major products by HPLC, confirming the absence of any significant side reactions. Without added Mg^{2+}, the composition of the (*S*)-**1a** sample declined from 94% to 69% (*S*)-**1a** upon irradiation for 1 h (black circles; Figure 3). In contrast, in the presence of Mg^{2+}, racemization was significantly inhibited, and the enantiomeric composition changed relatively little over the same time period (red squares; Figure 3).[18] This demonstrates that metal coordination correlates with suppression of photostereomutation in this aryl sulfoxide. As ϕ_f for **1a** increases from 0.01 to 0.35 in the presence of excess Mg^{2+}, this is consistent with metal ion coordination increasing fluorescence emission by suppressing excited state deactivation via pyramidal inversion.

An ICT Model for Excited State Pyramidal Inversion. It having been shown that metal ion mediated fluorescence enhancement correlates with suppression of photostereomutation, the next task was to explain why this should be so. It has long been known that photoracemization of aryl sulfoxides is far faster than thermal racemization,[12a,b] and that the barrier to excited state inversion must therefore be lower than the ground state barrier. As noted above, this reduction in inversion barrier is a singlet excited state process. However, a complete descriptive model has not previously been provided.[14]

The barrier to pyramidal inversion in sulfoxides is electrostatic in origin (Figure 4, left).[15] Increased repulsion between the lone pair electrons on S and O accounts for the higher energy of the planar configuration relative to the pyramidal configuration.

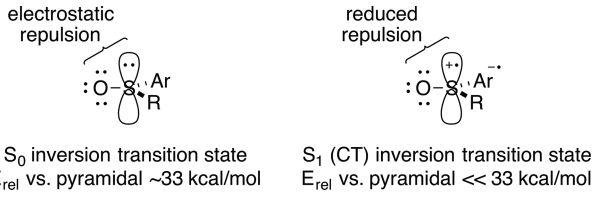

Figure 4. Origin of the inversion barriers in S_0 and S_1.

A simple explanation for rapid excited state pyramidal inversion would be that the planar sulfoxide transition state leading to inversion is a charge transfer (CT) state, in which electron density is shifted from the sulfoxide to the pyrene ring. This would presume initial excitation to a locally excited (LE) state, followed by intramolecular charge transfer (ICT) to form a lower energy CT state.

The resulting reduction in electron density at the sulfur center should lower the barrier to pyramidal inversion (Figure 4, right). This CT state would bear similarity to a sulfoxide radical cation, although (1) the molecule as a whole remains neutral and (2) the CT state formation does not necessarily involve complete transfer of an electron from the sulfoxide fragment to the pyrene ring. However, for convenience, we will discuss the proposed CT state as being a paired sulfoxide radical cation and pyrenyl radical anion.

In this CT model, pyramidal inversion would lead to enhanced nonradiative decay in the form of enhanced internal conversion (IC; Figure 5). Since the rate of IC scales with the negative exponent of ΔE,[19] the smaller S_0–S_1 separation in the planar transition state should lead to enhanced nonradiative decay.

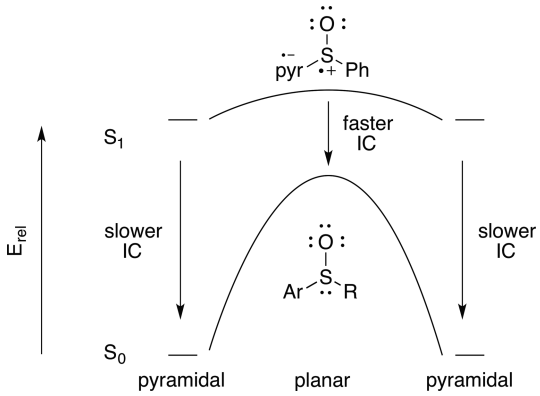

Figure 5. Enhanced internal conversion (IC) during pyramidal inversion in an intramolecular charge transfer (ICT) excited state (pyr = pyrene).

Fast $S_1 \rightarrow S_0$ IC at planar geometry would be followed by the return to either of the enantiomers, resulting in the observed rapid photostereomutation.

Existing support for this hypothesis comes in two forms. First, it has been established by pulse radiolysis and computational study that the methyl phenyl sulfoxide radical cation has the positive charge localized on S.[20a] Second, reversible $1e^-$ oxidation of enantiomerically enriched methyl phenyl sulfoxide leads to rapid racemization at room temperature, indicating low-barrier pyramidal inversion of the radical cation.[20b]

Additional support is provided by simulated photoelectron spectroscopy (PES) of phenyl pyrenyl sulfoxide in the gas phase (Figures S8, S9)[17] via accurate GW-BSE calculations.[21] The calculated optical absorption spectrum reveals a long wavelength electronic transition at 2.4 eV (~515 nm) that must be an $n \rightarrow \pi^*$ transition. Because it is symmetry-forbidden, it would be too weak to be observed directly in the UV spectrum, but would still represent direct transfer of an electron from a sulfoxide lone pair to the π^* orbital of pyrene. This is further confirmed by the theoretical analysis, which reveals the molecular states mainly contributing to this electronic excitation (Figure S9). The product of this excitation (sulfoxide radical cation/pyrenyl radical anion) would be the proposed CT state.

Substituent Effects. As a further test of the CT state hypothesis, we evaluated substituent effects on the spectroscopic properties of aryl sulfoxides by two approaches: first, exchanging the methyl group in **1a** for a phenyl group (**3a**; Chart 2), which facilitated electronic variation by substitution (**3b**,**c**); and, second, incorporating electron donating groups on the pyrene ring (**4**).[7]

Fluorophores with *p*-substituted phenyl groups were synthesized from bromopyrene (Scheme 2).[17] Lithiation of **5**

DOI: 10.1021/jacs.6b00572
J. Am. Chem. Soc. 2016, 138, 15889–15895

Chart 2. Substituted Aryl Sulfoxides

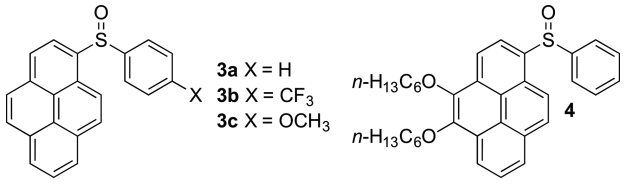

Scheme 2. Synthesis of 3a–c

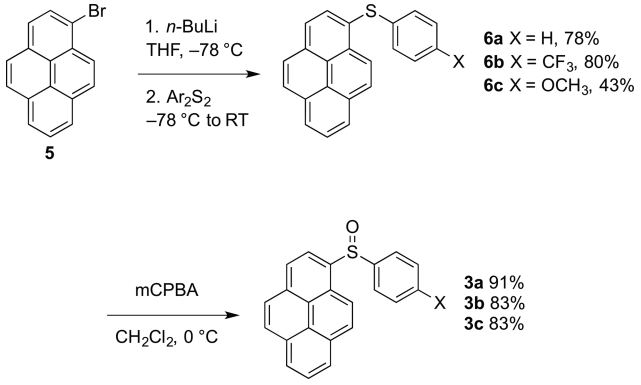

followed by reaction with appropriate disulfides gave the corresponding *p*-substituted phenyl pyrenyl sulfides **6a–c**. The sulfides were then oxidized to the sulfoxides (**3a–c**) with mCPBA in acceptable yield.

Sulfoxide **4** was synthesized from the dibromopyrene derivative **7** (Scheme 3).[17] Monolithiation of **7** followed by

Scheme 3. Synthesis of 4 (R = *n*-C_6H_{13})

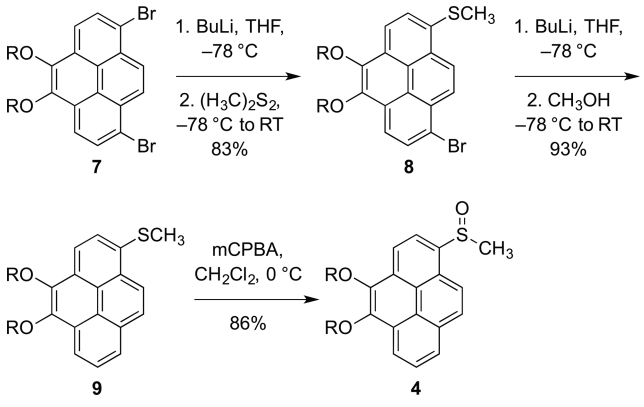

quenching with dimethyl disulfide provided intermediate **8** in 83% yield. Subsequent lithium–halogen exchange and quenching with CH_3OH gave compound **9** in 93% yield. Partial oxidation of this sulfide was carried out with mCPBA, furnishing sulfoxide **4** in 86% yield.

Spectroscopic properties such as extinction coefficients and excitation/emission maxima for **3a–c** were similar, and very similar to those of **1a–e**. However, fluorescence quantum yields (ϕ_f) varied significantly with *para* substitution: there is a 10-fold difference in ϕ_f between the *p*-OCH_3 and *p*-CF_3-substituted derivatives (**3b** vs **3c**). In parallel, the lifetimes (τ) of **3a–c** were observed to follow the same trend: a 10-fold change in τ is observed between **3b** and **3c**.

The extracted rates of radiative and nonradiative decay (k_r, k_{nr}; $k_r = \phi_f/\tau$; $k_{nr} = (1/\tau) - k_r$) are explanatory (Table 2). k_r

Table 2. Optical Properties of 3a–c[a]

	3a (*p*-H)	**3b** (*p*-CF_3)	**3c** (*p*-OCH_3)
λex/nm[b]	351	352	352
λem/nm[b]	380	381	379
$\varepsilon/10^3$ M^{-1} cm^{-1}	35.5	35.9	39.7
ϕ_f[c]	0.011	0.053	0.006
τ/ns	0.42	1.84	0.19
$k_r/10^8$ s^{-1}	0.24	0.29	0.32
$k_{nr}/10^8$ s^{-1}	21.5	5.15	53.7

[a]All measurements made in CH_3CN. Excitation/emission spectra acquired at 10^{-5} M. [b]Longest λ excitation/emission maxima. [c]Absolute quantum yields.

remains virtually independent of the *p*-substituent, although it is worth noting that the k_r are quite slow: on the order of 10^7 s^{-1}. In contrast, k_{nr} varies with substitution. The change from *p*-CF_3 to *p*-OCH_3 (**3b** vs **3c**) increases the rate of nonradiative decay by an order of magnitude, with the *p*-H (**3a**) value lying in between. As would be expected with near-invariant k_r, the k_{nr} values match the trends observed for ϕ_f and τ.

Substituent Effects Are Consistent with Deactivation via Pyramidal Inversion in a CT Excited State. The observed substituent effects are consistent with excited state deactivation by pyramidal inversion (Figures 4, 5). Previous studies have shown that the barrier for S_0 sulfoxide inversion is minimally perturbed by electronic effects.[22] In contrast, the variation (ca. 10-fold) in k_{nr} between **3b** and **3c** indicates stronger electronic effects for excited state stereomutation. This is reasonable, in that substituents on the phenyl ring are expected to influence the S_1 planar sulfoxide radical cation transition state more strongly than the uncharged S_0 planar sulfoxide transition state.[23] The electron withdrawing *p*-CF_3 group in **3b** should destabilize the fully conjugated, planar configuration of the sulfoxide radical cation (blue curve; Figure 6), whereas the electron donating *p*-OCH_3 group in **3c** should lead to stabilization (green curve; Figure 5). Therefore, the S_0–S_1 ΔE at planar geometry should vary with *p*-substituent as follows: OCH_3 < H < CF_3. This variance should be reflected in

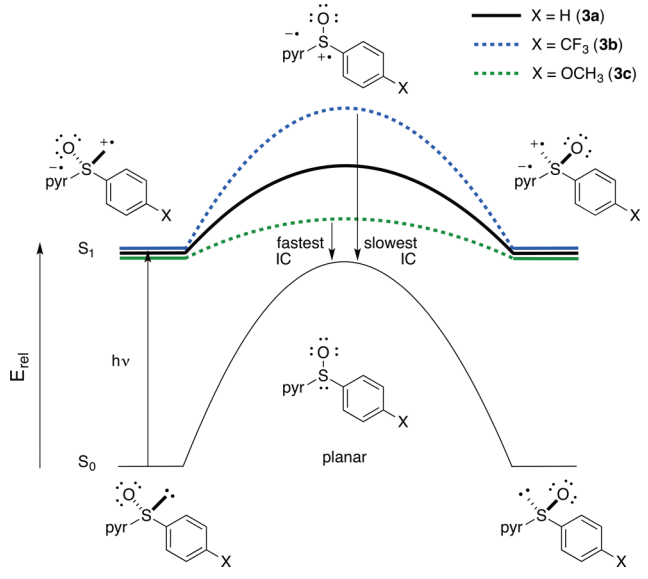

Figure 6. Qualitative potential energy (PE) diagram for electronic effects in **3a–c** (pyr = pyrene).

DOI: 10.1021/jacs.6b00572
J. Am. Chem. Soc. 2016, 138, 15889–15895

the rate of nonradiative IC between the planar S_0 and S_1 configurations, where the S_0−S_1 energy gap is the smallest, with IC being fastest for **3c** and slowest for **3b**. The measured quantum yields are in agreement with this analysis.

The high ϕ_f (0.43) of **4** relative to **1a** (0.012) can be rationalized by considering that the pyrene ring bearing OC_6H_{13} groups is electron rich in comparison to that of **1a**. Thus, formation of the CT sulfoxide radical cation/pyrenyl radical anion pair should be less favorable. This inhibition of CT state formation, and IC via pyramidal inversion, would lead to a higher ϕ_f.

Computational Characterization of the S_1 and S_0 Potential Energy Surfaces for 3a, with and without Mg^{2+}. The above indirect arguments are consistent with pyramidal inversion in a CT excited state determining the efficiency of nonradiative relaxation in S_1 of aryl sulfoxides. While complete energetic parameterization would be desirable, it is experimentally inaccessible. However, computational methods allow a quantitative analysis of the potential energy (PE) surfaces associated with **3a** (Table 3; Figures 6, 7).[17] Calculations were performed for the gas phase and with a CH_3CN continuum model. Discussion will focus on the CH_3CN calculations.[17]

Table 3. Calculated Ground and Excited State Inversion Barriers for 3a in the Gas and Solution Phases[a,b,17]

	gas phase	CH_3CN
3a (S_0)	36.2 (32.9)	36.0 (33.1)
3a (S_1)	5.04 (5.11)	5.56 (5.70)

[a] E_{rel}/kcal mol^{-1}. [b] Ground state calculations using B3LYP/Def2-TZVP (B97-D/Def2-TZVP); excited state calculations using TD-B3LYP/Def2-TZVP (TD-B97-D/Def2-TZVP//TD-B3LYP/Def2-TZVP).

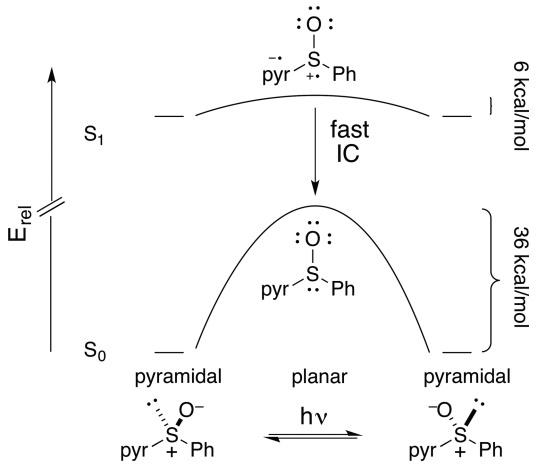

Figure 7. Simple potential energy diagram derived from calculated energetic data (in CH_3CN) for S_0 and S_1 of **3a** (pyr = pyrene).[15] See Table 3.

For ground state **3a**, the characteristic pyramidal structure is found, with a high barrier to pyramidal inversion via a planar transition state (Tables 3, S1, S2; Figures 7, S6, S7a). A pyramidal minimum energy structure for S_1 is also found, with an energy maximum at planar geometry (Tables 3, S1, S2; Figures 6, S6, S7a). However, the energy required to reach the planar geometry in S_1 is far lower than in S_0 (6 vs 36 kcal/mol).[17,24] At E_a = 6 kcal/mol, the rate for inversion should be on the order of 10^{11} s^{-1}, similar to the inversion barrier of an amine.[15] This reinforces the idea that the S_0−S_1 energy gap for the planar geometry allows a rate of IC that is fast on the time scale of radiative decay.

Upon further investigation (Table 4, Figure 8), it was determined that ground state effects play a only a minimal role

Table 4. Calculated Ground State Inversion Barriers for 3a·$MgCl_2$ in the Gas and Solution Phases[a,b,17]

	gas phase	CH_3CN
3a·$MgCl_2$ (S_0)	34.5	33.9

[a] E_{rel}/kcal mol^{-1}. [b] Calculated using B3LYP/Def2-TZVP.

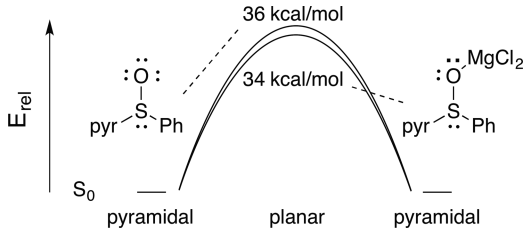

Figure 8. B3LYP/Def2-TZVP calculated S_0 inversion barriers (in CH_3CN) for **3a** and **3a**·$MgCl_2$ (pyr = pyrene; see also Table 4).[15]

in altering IC during pyramidal inversion. In CH_3CN, the ground state barrier to inversion of **3a**·$MgCl_2$ drops from 36.0 kcal/mol (**3a**) to 33.9 kcal/mol (ΔE_{rel} = 2 kcal/mol).[17] Thus, the observed increase in quantum yield induced by $MgCl_2$ addition (0.01 vs 0.35) is almost entirely an excited state effect.

Actinometry Reveals an Additional Dark Relaxation Pathway. As a final direct probe of the role of pyramidal inversion in the deactivation of S_1 for (*S*)-**1a**, we carried out chemical actinometry, using azoxybenzene as a reference,[25] in order to determine the total quantum yield for excited state pyramidal inversion.[17] By measuring the erosion of enantiomeric purity as a function of time under conditions where >99% of all photons are absorbed, and comparing this to Φ for the rearrangement of azoxybenzene under identical conditions, we find the total quantum yield for pyramidal inversion (Φ_{inv}) = 0.04 for (*S*)-**1a** (Figures S3, S4).[17] The maximum value for Φ_{inv} is 0.5, so pyramidal inversion accounts for only 8% of the excited state relaxation. Because ϕ_f for **1a** is 1%, this means that 91% of the absorbed photons remain unaccounted for. This in turn means that there must be another nonradiative relaxation pathway in addition to CT state pyramidal inversion.

An alternate process available to the CT excited state is the formation of a twisted intramolecular charge transfer state (TICT), in which the radical cation/radical anion pair is twisted fully out of conjugation.[26] TICT states are typically nonradiative because they lie above very high energetic maxima on the ground state PE surface, allowing for rapid IC. They are lower in energy than the parent CT state, primarily for steric reasons. Partitioning of the CT state between IC via pyramidal inversion and a TICT state that also undergoes rapid IC would account for the "missing" excited state energy (Figure 9).

An Alternate Role for Metal Ions in Enhancing Fluorescence. Taking together all of the above, we have been forced to rethink the basis for metal ion induced fluorescence in enhancement for aryl sulfoxides. While added metal ion should clearly suppress IC via pyramidal inversion in the CT state, it is not obvious how metal ions would suppress partitioning to a TICT state once the initial CT state is generated.

DOI: 10.1021/jacs.6b00572
J. Am. Chem. Soc. 2016, 138, 15889−15895

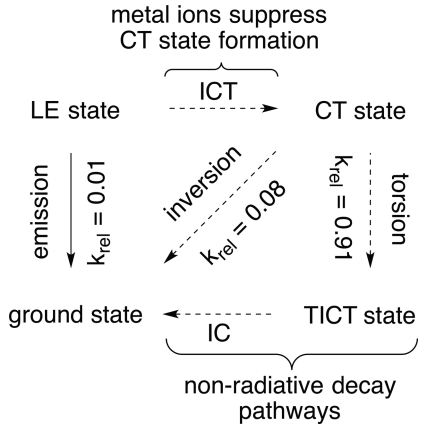

Figure 9. Proposed unifying scheme for excited state processes in aryl sulfoxides. Quantum yields used as a measure of k_{rel} for emission and inversion; k_{rel} for TICT formation inferred from these values. (See text.)

An alternative interpretation is inspired in part by the observation that **4**, the methyl pyrenyl sulfoxide with two alkoxy groups on the pyrene ring, is quite emissive (ϕ_f = 0.43). For **4**, we posited that the enhanced fluorescence was not caused by reduced pyramidal inversion, but rather by suppression of ICT and thus CT formation.

We believe that the simplest explanation for increased sulfoxide fluorescence in the presence of metal ions is that metal ion coordination to the sulfoxide oxygen withdraws enough electron density from the sulfoxide that ICT is suppressed, due to an increase of E_{rel} for the radical cation-like CT state. Upon blocking ICT, the two dominant nonradiative decay pathways (CT pyramidal inversion and TICT state formation) are both suppressed.

This interpretation is consistent with all of our experimental observations.

CONCLUSION

Through a combination of experimental and computational work, we have delineated a plausible mechanism for the function of aryl sulfoxide fluorescent chemosensors. A central conclusion is that the primary nonradiative decay pathways for these sulfoxides require formation of a CT excited state derived from the initially formed LE state. This CT state has radical cation character on the sulfoxide S atom, in which the sulfoxide has donated electron density to the pendant fluorophore. The addition of metal ions, which withdraw electron density from the sulfoxide upon coordination, suppresses formation of the CT state and leads to fluorescence enhancement.

It has previously been hypothesized that excited state pyramidal inversion is the dominant nonradiative relaxation pathway for aryl sulfoxides. We find that this pathway is relevant, and occurs in the CT state. However, the fate of aryl sulfoxide excited states is more complex than expected, and we have shown that there is an additional, dominant, nonradiative decay pathway that had not previously been recognized. We have proposed that this additional pathway is direct relaxation of a TICT state derived from the parent CT state.

These conclusions are supported experimentally and computationally, and this work represents the most complete model to date for excited state processes in aryl sulfoxides.

These data suggest that, for our next generation of fluorescent probes, electron deficient fluorophores, rather than the more common electron rich fluorescein-like fluorophores, e.g., should be explored, as this will facilitate the formation of the nonradiative CT state. This in turn will allow fluorescence to be "turned on" by the coordination of metal ions which block CT state formation. With this guidance in hand, we anticipate the development of improved chemosensors with broader application to biological and environmental problems.

ASSOCIATED CONTENT

Supporting Information

The Supporting Information is available free of charge on the ACS Publications website at DOI: 10.1021/jacs.6b00572.

Crystallographic data for (±)-**1a** and (*S*)-**1a** (CIF)
Experimental details, UV data, details of computational methods, and ^{1}H and ^{13}C NMR spectra (PDF)

AUTHOR INFORMATION

Corresponding Author

*nfinney@tju.edu.cn

ORCID

Anthony Linden: 0000-0002-9343-9180

Notes

The authors declare no competing financial interest.

ACKNOWLEDGMENTS

We thank the Department of Chemistry (University of Zurich), Research Priority Program LightChEC (University of Zurich), the School of Pharmaceutical Science and Technology (Tianjin University), the National Basic Research Program of China (2015CB856500), the Qian Ren Scholar Program of China, and the Synergetic Innovation Center of Chemical Science and Engineering (Tianjin University) for financial support. We thank Prof. Graham Bodwell (Memorial University of Newfoundland) for the generous gift of compound **7**.

REFERENCES

(1) Reviews on fluorescence-based molecular probes: (a) De Silva, A. P.; Gunaratne, H. N.; Gunnlaugsson, T.; Huxley, A. J.; McCoy, C. P.; Rademacher, J. T.; Rice, T. E. *Chem. Rev.* **1997**, *97*, 1515−1566. (b) Valeur, B.; Leray, I. *Coord. Chem. Rev.* **2000**, *205*, 3−40. (c) Bell, T. W.; Hext, N. M. *Chem. Soc. Rev.* **2004**, *33*, 589−598. (d) Callan, J. F.; De Silva, A. P.; Magri, D. C. *Tetrahedron* **2005**, *61*, 8551−8588. (e) Tsukanov, A. V.; Dubonosov, A. D.; Bren, V. A.; Minkin, V. I. *Chem. Heterocycl. Compd.* **2008**, *44*, 899−923. (f) Cho, D.-G.; Sessler, J. L. *Chem. Soc. Rev.* **2009**, *38*, 1647−1662. (g) Formica, M.; Fusi, V.; Giorgi, L.; Micheloni, M. *Coord. Chem. Rev.* **2012**, *256*, 170−192. (h) Li, X.; Gao, X.; Shi, W.; Ma, H. *Chem. Rev.* **2014**, *114*, 590−659.

(2) For overviews of PET-based fluorescent chemosensors, see: (a) Bissell, R. A.; de Silva, A. P.; Gunaratne, H. Q. N.; Lynch, P. L. M.; Maguire, G. E. M.; McCoy, C. P.; Sandanayake, K. R. A. S. *Top. Curr. Chem.* **1993**, *168*, 223−264. (b) de Silva, A. P.; Uchiyama, S. *Top. Curr. Chem.* **2010**, *300*, 1−28. For an overview of ICT signaling, and other approaches, see: (c) Demchenko, A. P. *Introduction to Fluorescence Sensing*; Springer Science: London, 2009; Chapter 6; see also ref 1.

(3) For rare examples of oxygen as the reporting element in fluorescent chemosensors, see: (a) Sousa, L. R.; Larson, J. M. *J. Am. Chem. Soc.* **1977**, *99*, 307−310. (b) De Silva, A. P.; Sandanayake, K. R. A. S. *J. Chem. Soc., Chem. Commun.* **1989**, 1183−1185. (c) Wallace, K. J.; Fagbemi, R. I.; Folmer-Andersen, F. J.; Morey, J.; Lynth, V. M.; Anslyn, E. V. *Chem. Commun.* **2006**, 3886−3888.

(4) For fluorescent probes based on phosphorus oxidation, see: (a) Akasaka, K.; Suzuki, T.; Ohrui, H.; Meguro, H. *Anal. Lett.* **1987**,

DOI: 10.1021/jacs.6b00572
J. Am. Chem. Soc. 2016, 138, 15889−15895

20, 731−745. (b) Lemieux, G. A.; de Graffenried, C. L.; Bertozzi, C. R. *J. Am. Chem. Soc.* **2003**, *125*, 4708−4709. (c) Onoda, M.; Uchiyama, S.; Endo, A.; Tokuyama, H.; Santa, T.; Imai, K. *Org. Lett.* **2003**, *5*, 1459−1461. (d) Soh, N.; Sakawaki, O.; Makihara, K.; Odo, Y.; Fukaminato, T.; Kawai, T.; Irie, M.; Imato, T. *Bioorg. Med. Chem.* **2005**, *13*, 1131−1139. (e) Onoda, M.; Tokuyama, H.; Uchiyama, S.; Mawatari, K.-I.; Santa, T.; Kaneko, K.; Imai, K.; Nakagomi, K. *Chem. Commun.* **2005**, 1848−1850. (f) Soh, N.; Ariyoshi, T.; Fukaminato, T.; Nakajima, H.; Nakano, K.; Imato, T. *Org. Biomol. Chem.* **2007**, *5*, 3762−3768.

(5) For fluorescent chemosensors based on sulfur manifested in a thiourea moiety, see: (a) Mello, J. V.; Finney, N. S. *J. Am. Chem. Soc.* **2005**, *127*, 10124−10125. (b) Malashikhin, S. A.; Baldridge, K. K.; Finney, N. S. *Org. Lett.* **2010**, *12*, 940−943. (c) Profatilova, I. A.; Bumber, A. A.; Tolpygin, I. E.; Rybalkin, V. P.; Gribanova, T. N.; Mikhailov, I. E. *Russ. J. Gen. Chem.* **2005**, *75*, 1774−1781. (d) Tolpygin, I. E.; Shepelenko, E. N.; Revinskii, Y. V.; Tsukanov, A. V.; Dubonosov, A. D.; Bren, V. A.; Minkin, V. I. *Russ. J. Gen. Chem.* **2010**, *80*, 765−770. (e) Li, X. L.; He, Y. W.; Yang, S. I. *Bull. Korean Chem. Soc.* **2011**, *32*, 338−340. (f) Vonlanthen, M.; Finney, N. S. *J. Org. Chem.* **2013**, *78*, 3980−3988. (g) Vonlanthen, M.; Connelly, C. M.; Deiters, A.; Linden, A.; Finney, N. S. *J. Org. Chem.* **2014**, *79*, 6054−6060. For fluorescent probes relying on the oxidation state of sulfur, see: (h) Malashikhin, S.; Finney, N. S. *J. Am. Chem. Soc.* **2008**, *130*, 12846−12847. (i) Dane, E. L.; King, S. B.; Swager, T. M. *J. Am. Chem. Soc.* **2010**, *132*, 7758−7768. (j) Marom, H.; Popowski, Y.; Antonov, S.; Gozin, M. *Org. Lett.* **2011**, *13*, 5532−5535.

(6) For fluorescent probes relying on bonding with arsenic, see: (a) Griffin, B. A.; Adams, S. R.; Tsien, R. Y. *Science* **1998**, *281*, 269−272. (b) Adams, S. R.; Campbell, R. E.; Gross, L. A.; Martin, B. R.; Walkup, G. K.; Yao, Y.; Llopis, J.; Tsien, R. Y. *J. Am. Chem. Soc.* **2002**, *124*, 6063−6076. (c) Scheck, R. A.; Schepartz, A. *Acc. Chem. Res.* **2011**, *44*, 654−665.

(7) Kathayat, R. S.; Finney, N. S. *J. Am. Chem. Soc.* **2013**, *135*, 12612−12614.

(8) For reviews on sulfoxide metal coordination, see: (a) Calligaris, M.; Carugo, O. *Coord. Chem. Rev.* **1996**, *153*, 83−154. (b) Calligaris, M. *Coord. Chem. Rev.* **2004**, *248*, 351−375.

(9) The crystal structure of $Mg^{2+}\cdot(H_2O)_2(DMSO)_6$ shows exclusive coordination through the sulfoxide oxygen. See: Ullström, A.-S.; Warminska, D.; Persson, I. *J. Coord. Chem.* **2005**, *58*, 611−622 In addition, as noted in ref 8b, sulfoxide S-coordination has only been observed for late transition metals, and alkaline and alkaline earth cation complexes have only been found in O-coordinated form.

(10) (a) Celebre, G.; Cinacchi, G.; De Luca, G.; Giuliano, B. M.; Iemma, F.; Melandri, S. *J. Phys. Chem. B* **2008**, *112*, 2095−2101. (b) Buchanan, G. W.; Reyes-Zamora, C.; Clarke, D. E. *Can. J. Chem.* **1974**, *52*, 3895−3904.

(11) The shift of the longest wavelength λ_{max} from 335 to 350 nm represents a π/π^* energy gap change of only 3 kcal/mol.

(12) For fundamental studies on the photochemistry of aryl sulfoxides, see: (a) Mislow, K.; Axelrod, M.; Rayner, D. R.; Gotthardt, H.; Coyne, L. M.; Hammond, G. S. *J. Am. Chem. Soc.* **1965**, *87*, 4958−4959. (b) Guo, Y.; Jenks, W. J. *J. Org. Chem.* **1997**, *62*, 857−864. (c) Lee, W.; Jenks, W. S. *J. Org. Chem.* **2001**, *66*, 474−480. (d) Cubbage, J. W.; Jenks, W. S. *J. Phys. Chem. A* **2001**, *105*, 10588−10595. (e) Vos, B. W.; Jenks, W. S. *J. Am. Chem. Soc.* **2002**, *124*, 2544−2547.

(13) Berlman, I. *Handbook of Fluorescence Spectra of Aromatic Molecules*; Academic Press: New York, 1971.

(14) For an elegant, early computational study of pyramidal inversion in the excited states of DMSO and H_2SO, see ref 12d.

(15) For fundamental discussions of pyramidal inversion, see: (a) Rauk, A.; Allen, L. C.; Mislow, K. *Angew. Chem., Int. Ed. Engl.* **1970**, *9*, 400−414. (b) Baechler, R. D.; Andose, J. D.; Stackhouse, J.; Mislow, K. *J. Am. Chem. Soc.* **1972**, *94*, 8060−8065.

(16) (a) Legros, J.; Bolm, C. *Chem.-Eur. J.* **2005**, *11*, 1086−1092. (b) Drago, C.; Caggiano, L.; Jackson, R. F. W. *Angew. Chem., Int. Ed.* **2005**, *44*, 7221−7223.

(17) See Supporting Information for details.

(18) We believe that the small amount of photoracemization in the presence of Mg^{2+} is the result of inversion in free **1a**, as the experiment was carried out in the presence of ∼100 equiv of Mg^{2+}. It takes ∼10,000 equiv of Mg^{2+} to saturate formation of $Mg^{2+}\cdot$**1a** at [**1a**] = 10^{-5} M. See ref 7.

(19) For leading references, see: (a) Freed, K. F. *Acc. Chem. Res.* **1978**, *11*, 74−80. (b) Klessinger, M.; Michl, J. *Excited States and Photochemistry of Organic Molecules*; VCH: New York, 1995; pp 252−260. The use of the term photoracemization instead of photostereomutation is preferred in this case, as racemization of (*S*)-**1a** is being discussed.

(20) (a) Baciocchi, E.; Del Giacco, T.; Gerini, M. F.; Lanzalunga, O. *J. Phys. Chem. A* **2006**, *110*, 9940−9948. Notably, these calculations consistently find a pyramidal configuration of the radical cation as the minimum on the excited state potential energy surface. E_a for pyramidal inversion of the ground state radical cation is estimated to be ∼11 kcal/mol, compared to the inversion of the neutral sulfoxide (∼33 kcal/mol). Further, a low reorganization energy is observed for $1e^-$ oxidation of $PhS(O)CH_3$, suggesting a radical cation geometry very similar to that of the tetrahedral ground state. See: (b) Aurisicchio, C.; Baciocchi, E.; Gerini, M. F.; Lanzalunga, O. *Org. Lett.* **2007**, *9*, 1939−1942.

(21) Hybertsen, M. S.; Louie, S. G. *Phys. Rev. B: Condens. Matter Mater. Phys.* **1986**, *34*, 5390−5413.

(22) The rate of thermal pyramidal inversion of *p*-substituted aryl sulfoxides varies by a factor of less than two with variation of the substituents at the *p*-position. See: Rayner, D. R.; Gordon, A. J.; Mislow, K. *J. Am. Chem. Soc.* **1968**, *90*, 4854−4860.

(23) At the planar configuration, the S-atom in the excited state can be described as sp^2-hybridized, with a partially filled p orbital. This hybridization should lead to enhanced π-conjugation with the neighboring aromatic rings compared to the ground state. This explains the fact that substituent effects in the excited state are larger than those in the ground state.

(24) Although early computational studies suggested that the planar configuration was a minimum on the excited state potential energy surface (ref 12d), our calculations at more recently available levels of theory consistently find that the minimum energy configuration of the excited state is pyramidal. See also ref 20.

(25) Bunce, N. J.; LaMarre, J.; Vaish, S. P. *Photochem. Photobiol.* **1984**, *39*, 531−533.

(26) (a) Grabowski, Z. R.; Rotkiewicz, K.; Rettig, W. *Chem. Rev.* **2003**, *103*, 3899−4032. (b) Sasaki, S.; Drummen, G. P. C.; Konishi, G.-i. *J. Mater. Chem. C* **2016**, *4*, 2731−2743.

DOI: 10.1021/jacs.6b00572
J. Am. Chem. Soc. 2016, 138, 15889−15895